JACS
JOURNAL OF THE AMERICAN CHEMICAL SOCIETY
Article
pubs.acs.org/JACS

Tin(II) Sulfide (SnS) Nanosheets by Liquid-Phase Exfoliation of Herzenbergite: IV–VI Main Group Two-Dimensional Atomic Crystals

Jack R. Brent,[†,∥] David J. Lewis,[*,†,‡,∥] Tommy Lorenz,[§] Edward A. Lewis,[†] Nicky Savjani,[‡] Sarah J. Haigh,[†] Gotthard Seifert,[*,§] Brian Derby,[*,†] and Paul O'Brien[*,†,‡]

[†]School of Materials and [‡]School of Chemistry, University of Manchester, Oxford Road, Manchester, M13 9PL, United Kingdom
[§]Theoretische Chemie, Technische Universität Dresden, 01069 Dresden, Germany

Supporting Information

ABSTRACT: The liquid-phase exfoliation of tin(II) sulfide to produce SnS nanosheets in *N*-methyl-2-pyrrolidone is reported. The material is characterized by Raman spectroscopy, atomic force microscopy, lattice-resolution scanning transmission electron microscope imaging, and energy dispersive X-ray spectrum imaging. Quantum chemical calculations on the optoelectronic characteristics of bulk and 10-layer down to monolayer SnS have been performed using a quantum chemical density functional tight-binding approach. The optical properties of the SnS and centrifugally fractionated SnS nanosheet dispersions were compared to that predicted by theory. Through centrifugation, bilayer SnS nanosheets can be produced size-selectively. The scalable solution processing of semiconductor SnS nanosheets is the key to their commercial exploitation and is potentially an important step toward the realization of a future electronics industry based on two-dimensional materials.

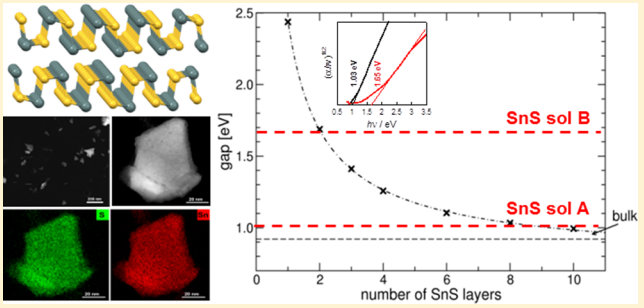

INTRODUCTION

Orthorhombic tin(II) sulfide (SnS, Herzenbergite)[1] is a binary main group chalcogenide that has recently attracted interest because it is a semiconductor. The crystal structure of Herzenbergite (Figure 1) is a layered structure of strong Sn–S bonds within a puckered *a*–*b* sheet with weak intermolecular interactions between the layers[2] that is similar in structure to that of black phosphorus,[3] with which it is isoelectronic. SnS is relatively nontoxic, comprised of earth abundant elements, and has an indirect band gap[4] similar in energy to silicon with a large absorbance coefficient ($\alpha > 10^4$) across the ultraviolet, visible, and near-infrared regions of the electromagnetic spectrum, making it potentially useful for photovoltaic (PV) applications. The indirect optical band gap in SnS requires the active layer of PV devices manufactured from the material to be relatively thick, though the intrinsic ability of the indirect band gap to suppress direct recombination of excitons by photoluminescence confers the advantage of increased PV power conversion efficiency. Current champion solar cells which include SnS as the intrinsic semiconductor/absorber layer have power conversion efficiencies of 4.4%,[5] with a theoretical maximum of 24% predicted.[6] We have reported the synthesis of SnS thin films using aerosol-assisted chemical vapor deposition (AACVD) from dithiocarbamato-tin(II) and organotin(IV) complexes.[7,8] Other strategies toward SnS thin films include conventional CVD,[9−15] chemical bath deposition,[16,17] electrochemical deposition,[18,19] chemical vapor transport,[20,21] atomic layer deposition,[22,23] spray pyrolysis,[24−26] and dip deposition.[27] Synthetic routes toward SnS nanoparticles are generally based around solution thermolysis of precursors.[28−35] A recent review of synthetic strategies toward SnS (as well as SnSe, SnTe, and Cu_2ZnSnS_4 "CZTS") thin films and nanoparticles is available.[36]

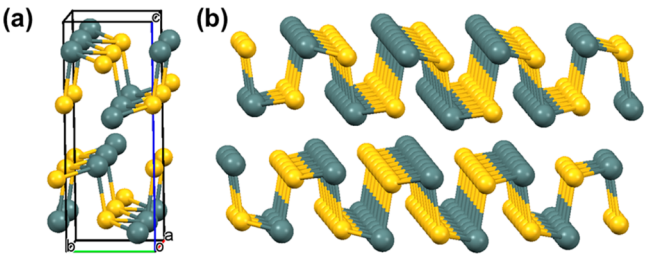

Figure 1. Crystal structures of the compounds described in this study. (a) The orthorhombic unit cell of Herzenbergite, tin(II) sulfide (a = 3.98 Å; b = 4.33 Å; c = 11.18 Å; $\alpha = \beta = \gamma = 90°$; space group *Pmcn*; Crystallography Open Database ID: 1011253) which generates corrugated layers of SnS held together by weak interlayer forces. (b) A SnS bilayer nanosheet viewed close to the [100] direction, i.e., parallel to the sheets.

Two-dimensional (2-D) materials are a recently established class of materials.[37] The archetypal material, graphene, consists of an atomically thin layer of sp^2 hybridized carbon atoms.[38] Similarly, 2-D binary transition-metal dichalcogenides (TMDCs) such as molybdenum disulfide (MoS_2)[39] and

Received: August 5, 2015
Published: September 9, 2015

DOI: 10.1021/jacs.5b08236
J. Am. Chem. Soc. 2015, 137, 12689−12696

tungsten disulfide (WS_2) have been prepared.[40] The thinning of layered bulk materials to their 2-D variants often has consequences such as improved mechanical,[41] conductive,[42] and optoelectronic properties[43] compared with the parent bulk materials. The search for 2-D materials beyond graphene is ongoing,[44] and recently a phosphorus analogue of graphene, so-called phosphorene,[45,46] which is a 2-D atomic crystal of orthorhombic black phosphorus, has attracted major interest from materials scientists and physicists due to its narrow and tunable band gap (bulk $E_g \approx 0.3$ eV, monolayer $E_g \approx 1$ eV) and high hole mobility (monolayer $\mu \approx 1000$ cm^2 V s^{-1}), bridging the band gap and carrier mobility discrepancy between graphene (zero band gap, high carrier mobility $\mu > 10^6$ cm^2 V s^{-1}) and 2-D TMDCs (wide band gap $E_g \approx 2.0$ eV, low carrier mobility $\mu \approx 100$ cm^2 V s^{-1}) as well as having various anisotropic optoelectronic[47] and mechanical properties.[48] However, questions remain concerning the stability of phosphorene with respect to oxidation to phosphoric acids, which has led researchers to pursue various strategies to stabilize the material including encapsulation in aluminum oxide,[49] hexagonal boron nitride (h-BN),[50] or, in the case of liquid-exfoliated material, sterically hindered solvents.[51] The mechanism of degradation still remains unclear, and thus unanswered questions loom regarding the future use of the material.

There are a number of approaches toward the synthesis of 2-D materials. Micromechanical exfoliation (so-called Scotch tape delamination) can be used to produce large flakes of 2-D materials including, but not limited to, graphene, 2-D TMDCs, and phosphorene.[45] The method is useful for producing small amounts of large, high-quality pristine nanosheets but requires suitable large size starting crystals and is obviously not scalable. Circumventing the scale up problem, CVD methods have been developed to grow large-area graphene[52] and TMDCs.[53] Potentially, the most useful method for producing nanosheets on a large scale is liquid-phase exfoliation. In the latter method, the bulk layered crystal is placed in a liquid selected for its capability of solvating the 2-D material,[54,55] typically *N*-methyl-2-pyrrolidone (NMP), and the layered materials are forced apart by ultrasonic excitation to form stable, crystalline nanosheet dispersions.[56−58] Recently, shear exfoliation in liquids containing detergents has been demonstrated as a large-scale method for the production of a range of 2-D materials including graphene and MoS_2.[59,60] Thus, liquid-phase exfoliation has great potential for the scaled up manufacture of 2-D materials, essential to a future electronics industry based on 2-D devices. We have recently reported the liquid-phase exfoliation of MoS_2 from molybdenite ores,[61] Cr-doped MoS_2 nanosheets from AACVD-grown alloys,[62] and few-layer phosphorene from black phosphorus.[63] Phosphorene produced by liquid-phase exfoliation of black phosphorus can potentially be of electronics grade quality.[64,65]

Group IV−VI SnS nanosheets are isoelectronic with phosphorene (Figure 1b) as hexagonal boron nitride is to graphene and indeed should offer the tunable bandgap benefits of phosphorene as well as possessing anisotropic optoelectronic and mechanical properties, while displaying potentially superior stability compared with the elemental group V 2-D material. SnS nanosheets have previously been produced by mainly bottom-up methods, though generally are not few-layered materials, and there is a consistent lack of analysis regarding the thicknesses of the nanosheets reported so far,[29,32,66−70] although an interesting bottom-up synthesis of isoelectronic (though structurally unrelated) ultrathin PbS nanosheets has been reported by Acharya and co-workers.[71] In this paper we report the synthesis of few-layer SnS nanosheets by liquid-phase exfoliation. The synthesis is scalable and thus complements the range of materials that may be presently produced by liquid-phase exfoliation. The nanosheets are fully characterized by a range of spectroscopic and microscopic analyses, the optical band gap of exfoliated nanosheets is evaluated, and quantum chemical calculations are presented that marry experiment to theory. The synthesis of stable colloidal SnS nanosheets reported here represents an important step to the realization of 2-D inks based on SnS, which may potentially be suitable for screen printing, slot die coating, roll-to-roll processing, or inkjet printing onto flexible substrates.

EXPERIMENTAL SECTION

General. Tin(II) sulfide and NMP were purchased from Sigma-Aldrich. All solvents were degassed prior to use.

Instrumentation. Raman spectra were measured using a Renishaw 1000 Micro-Raman System equipped with a 514 nm laser operating at 1 mW. Atomic force microscopy (AFM) was performed using a Bruker Multimode 8 instrument equipped with a Bruker SCANASYST-AIR silicon nitride cantilever tip with a nominal radius of 2 nm operating under ambient conditions in PeakForce quantitative nanomechanical mapping (QNM) mode at a scan rate of 0.5 Hz and 512 samples per line. Samples analyzed by scanning transmission electron microscopy (STEM) were prepared by drop casting dispersions of nanosheets in NMP onto lacey carbon grids. Between drop casting and imaging, samples were stored under vacuum. High-angle annular dark-field (HAADF) STEM imaging and energy dispersive X-ray (EDX) spectrum imaging were performed using a probe side aberration corrected FEI Titan G2 80−200 S/TEM ChemiSTEM instrument operated at 200 kV with a probe current of ∼440 pA, a probe convergence angle of 21 mrad, and a HAADF inner angle of 54 mrad. EDX spectroscopy data was acquired with all four detectors on, and the sample untilted EDX spectra and spectrum images were analyzed using Bruker Esprit software, and STEM images were analyzed using Gatan Digital Micrograph and ImageJ software. Mercury or Crystalmaker software were used to generate crystal structures. UV−vis-NIR spectra were recorded using a PerkinElmer Lambda 1050 instrument, with diluted sols in NMP using quartz cuvettes with a path length of 1 cm.

Exfoliation Procedure. Tin(II) sulfide (363 mg) was added to degassed NMP (15 mL) in an argon-flushed vial and sealed tightly with a lid and the edges of the lid wrapped with parafilm. The suspensions were ultrasonicated in an Elmasonic P 70H benchtop ultrasonic bath (820 W across four horns) operating at 37 kHz frequency and 30% power for 24 h. The bath was modified by the addition of a water-cooling coil to maintain the water temperature below 30 °C during sonication.

Purification of SnS nanosheets (SnS Sol A). Upon completion of the exfoliation step, an aliquot (5 mL) was removed and diluted with NMP (5 mL). The dispersion was centrifuged (Centurion 822 series benchtop centrifuge) at a rate of 1500 rpm (relative centrifugal force ∼180 *g*) for 45 min to remove the remaining bulk material. The top two-thirds of the supernatant was collected for analysis. An aliquot of the dispersion was spin-coated at 6000 rpm onto 300 nm SiO_2 on Si substrates using a spin coater (Ossila, U.K.) for further analysis.

Isolation of Bilayer SnS Nanosheets (SnS Sol B). To further fractionate the solution and isolate bilayer SnS nanosheets, a portion (ca. 5 mL) of SnS Sol A was centrifuged (Thermo Scientific HERAUS Multifuge X1 Centrifuge) at 10,000 rpm (relative centrifugal force ∼11620 *g*) for 40 min. Half of the resulting supernatant was pipetted to provide a suspension of bilayer SnS nanosheets in NMP. An aliquot the dispersion was spin-coated at 6000 rpm onto 300 nm SiO_2 on Si substrates using a spin coater (Ossila, U.K.) for further analysis.

Computational Analysis. A density functional tight-binding (DFTB)[72−76] method was used for the calculation of the band

DOI: 10.1021/jacs.5b08236
J. Am. Chem. Soc. 2015, 137, 12689−12696

structures as well as the densities of states, band gaps, energies, and absorption spectra. It is based on the density functional theory (DFT) of Hohenberg and Kohn[77] in the formulation of Kohn and Sham.[78] The Kohn–Sham orbitals $\psi_i(\vec{R})$ are expanded in a set of atom-centered basis functions $\varphi_j(\vec{R})$. These functions are determined by self-consistent density functional calculations on the isolated atoms employing a large set of Slater-type basis functions.

The effective one-electron potential in the Kohn–Sham Hamiltonian is approximated as a superposition of the potentials of neutral atoms. Moreover, only one- and two-center integrals are calculated to set up the Hamilton matrix. We have taken a minimal valence basis including the 3s, 3p, and 3d orbitals for sulfur and the 5s, 5p, and 5d orbitals for tin including scalar relativistic effects. Spin–orbit coupling has not been considered because previous publications show that the influence on the band gap is <0.1 eV.[79] States below these levels were treated within a frozen-core approximation. All calculations were performed using rectangular periodic boundary conditions in the program packages Dylax and an experimental version of the deMon code with a DFTB and linear response implementation.[80] For comparison, the band structures have been calculated also with DFT using a PBE exchange–correlation functional[81] with a DZP (double-ζ-polarization contracted Gaussian basis set) basis as implemented in the Siesta[82] program package; rectangular periodic boundary conditions were applied.

The band gap energies of the bulk phase, single, and multilayers were obtained from the band structures which have been calculated for the primitive cells[83] along all symmetry lines and the absorption spectra which have been calculated for rectangular supercells with in-plane edge-lengths of approximately 20 Å. For the density of states (DOS) calculations a set of 8 × 8 × 8 and 8 × 8 × 1 optimized Monkhorst–Pack *k*-points[84] were used for the bulk and layers, respectively. Absorption spectra were calculated by using the time-dependent linear response theory and the Γ point approximation. The crystal structure of the SnS bulk phase was obtained from Wiedemeier et al.[83] The structures of the single and multilayers have been derived from this bulk structure without any further geometry optimization.

RESULTS AND DISCUSSION

Synthesis and Characterization. Herzenbergite (SnS) is a main group chalcogenide mineral that possesses a layer structure (Figure 1a) of puckered SnS layers, held together by weak interlayer forces. It is essentially an isoelectronic IV–VI analogue of black phosphorus, with similar crystal packing. As with other layered materials, it was expected that liquid-phase exfoliation of Herzenbergite could potentially lead to the formation of SnS nanosheets, thinned to the nanometer scale along the [001] direction (*c*-axis direction of the SnS unit cell). Ultrasonic exfoliation of Herzenbergite in NMP over a period of 24 h, followed by centrifugation to remove unexfoliated bulk material led to the formation of turbid brown solutions (henceforth referred to as SnS sol A) which were further analyzed by Raman spectroscopy, AFM, and STEM. Further centrifugation of SnS sol A led to a so-called "fractionated" sol (henceforth referred to as SnS sol B) that contained SnS sheets thinned to near atomic dimensions (*vide infra*).

Exfoliated nanosheets from SnS sol A were spin-coated onto silicon substrates, and height-profiling was performed using AFM (Figure 2a). In total, 141 nanosheets were analyzed (N = 141) to generate particle size distributions of %N as a function of nanosheet height (Figure 2c), where the height is the distance measured of the crystallographic *c* axis and thus can be considered the thickness of the sheets. The nanosheets in SnS sol A were revealed to have polydisperse thicknesses up to 15 nm, with a mean thickness of 7.8 ± 2.5 nm. However, nanosheets in SnS sol B were revealed to be almost monodisperse in thickness, with a Gaussian-like particle

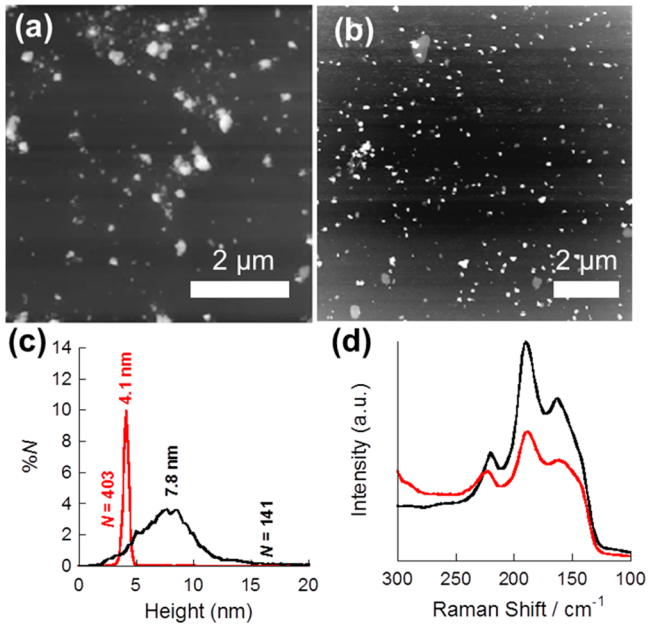

Figure 2. Characterization of liquid-phase exfoliated SnS nanosheets. (a) Representative wide-area AFM height profile image of few-layer SnS sol A nanosheets produced from ultrasonic exfoliation of Herzenbergite SnS in NMP for 24 h and spin-coated onto a 300 nm Si@SiO_2 substrate. The scale bar represents 2 μm. (b) Representative wide-area AFM height profile image of SnS sol B nanosheets produced from centrifugation of SnS sol A and spin-coated onto a 300 nm Si@SiO_2 substrate. The scale bar represents 2 μm. (c) Particle size distribution for nanosheet height as determined for SnS sol A (black curve, N = 141) and SnS sol B (red curve, N = 403), with mean sheet thickness for both. (d) Raman spectra of SnS sol A (black curve) and SnS sol B (red curve), both spin-coated onto a 300 nm Si@SiO_2 substrates.

number distribution and a mean nanosheet thickness of 4.1 ± 0.24 nm, or around 3–4 SnS bilayers based on the calculation 4.1/1.18 nm, where the denominator is taken as the *c* axis of the SnS crystal structure presented in Figure 1, assuming the unit cell includes a single SnS bilayer. However, we note that this is likely to be an overestimation of the thickness in terms of SnS layers since solution-processed 2-D crystals are known to include a ∼1 nm overlayer of the solvent that the exfoliation was performed in when deposited on a substrate.[85−87] Indeed, when this is considered along with that the shortest layer-to-layer separation[2] inclusive of a single SnS monolayer in the [001] direction of SnS is ca. 0.9 nm (Supporting Information), it suggests that sheets with ca. 4 nm thickness are comprised of fewer layers than expected and that division of the height thickness found by AFM by the crystallographic dimensions to obtain the number of atomic layers in a nanosheet is potentially inaccurate. The discrepancy between AFM and predicted height from crystallography for a 2-D material with a similar corrugated crystal structure has been observed previously with black phosphorus, which adopts a similar crystal structure to SnS; Coleman and co-workers have suggested that the height of solution-processed black phosphorus monolayers is 2 nm per layer from AFM,[51] presumably because of adsorption of cyclohexyl-2-pyrrolidone molecules on the surface of exfoliated flakes. The latter monolayer measurement is much larger than that predicted by the black phosphorus crystal structure,[3] where c = 1.05 nm (includes 2 sheets per cell), but is highly reproducible. In the

DOI: 10.1021/jacs.5b08236
J. Am. Chem. Soc. 2015, 137, 12689–12696

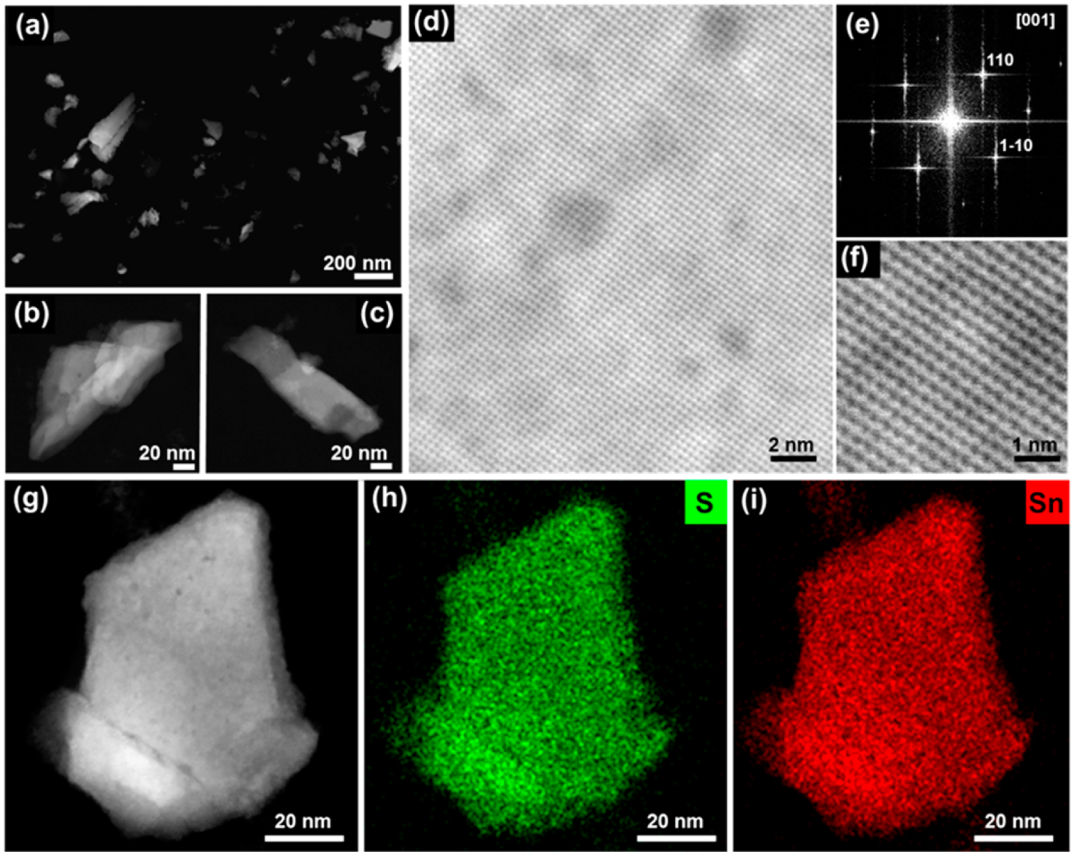

Figure 3. Characterization of representative SnS nanosheets by electron microscopy. (a) Low resolution HAADF STEM image showing typical sizes of SnS nanosheets as an ensemble. Scale bar represents 200 nm. (b and c) HAADF STEM images of typical SnS nanosheets. Scale bars represent 20 nm. (d) Atomic resolution HAADF STEM image of a typical region of a crystalline SnS nanosheet. Scale bar represents 2 nm. (e) The Fourier transform from the same region of the nanosheet as in (d), indexed along the [001] direction of the SnS unit cell. (f) An higher magnification HAADF STEM image of the same region of the nanosheet in (d). Scale bar represents 1 nm. (g) HAADF STEM image of a single SnS nanosheet. Scale bar represents 20 nm. (h and i) EDX spectrum imaging of the same nanosheet as in (g), showing the even distribution of sulfur and tin throughout the nanosheet. Scale bars represent 20 nm.

case of Scotch tape exfoliated monolayer black phosphorus, the overestimation is less due to the lack of adsorbed molecules but still significant (ca. 0.2 nm overestimated as 0.9 nm by AFM).[45] Conjecture that solution-processed SnS also manifests the same artifact by AFM is supported when optical absorption measurements and DFTB calculations on the SnS sol B are considered (*vide infra*). It is most likely that SnS sol B predominantly consists of bilayer SnS nanosheets based on a "corrected" value of 2 nm/layer from solution processed black phosphorus and a mean height of 4.1 nm.[51]

Raman spectroscopy was used to investigate the nanosheets further with comparison to bulk SnS (Figure 2d). Bulk SnS has 12 Raman active bands ($4A_g$, $2B_{1g}$, $4B_{2g}$, and $2B_{3g}$). Due to the anisotropic nature of the SnS crystal structure, the direction of the incident radiation dictates the phonon modes that are observed for single crystals cleaved in the *c*-plane for instance.[88] For randomly orientated bulk crystallites, all phonon modes should in theory be observed simultaneously. Hence, for 2-D thinned material, the Raman spectrum should change dramatically compared to the Raman spectrum of the bulk material. The Raman spectrum of bulk SnS on a silicon substrate displays two broad bands with peak maxima at 153 and 220 cm^{-1} (Supporting Information).[89] The small peak at 294 cm^{-1} is tentatively assigned to a shift of the B_{2g} optical mode in bulk SnS. The Raman spectrum of SnS sol A spin-coated onto a silicon substrate, on the other hand, revealed sharpened bands with peak maxima at 164, 190, and 220 cm^{-1}, which can be tentatively assigned to the B_{3g}, A_g, and B_{3u} optical modes, suggesting that thinning of the bulk material in the [001] direction has a significant impact on the optical modes as-observed by Raman spectroscopy. The sharpening of the bands in the Raman spectrum in SnS nanosheets compared to the broad bulk profile has been observed previously in SnS nanosheets prepared by laser ablation.[90] The Raman spectrum of SnS sol B nanosheets consists of similar features compared with SnS sol A, although the B_{3g}, A_g, and B_{3u} optical modes appear slightly shifted at 162, 189, and 224 cm^{-1}. Shifts in the positions of optical Raman bands when bulk materials are thinned to 2-D materials is a well-established phenomenon.[91]

The nanosheets produced from liquid-phase exfoliation of SnS Herzenbergite were further investigated by STEM. Low-magnification HAADF STEM images (Figure 3a–c) show that the nanosheets are typically 50–100 nm in lateral dimension often with aspect ratios of around 1.5–2.0, suggesting that exfoliation is potentially anisotropic with respect to the *a* and *b* crystallographic axes, possibly not surprising for a material that shows structural anisotropy in the *ab* plane. Atomic resolution HAADF STEM imaging demonstrates the highly crystalline nature of the nanosheets that appear largely defect-free. Fourier transformation of the atomic resolution HAADF STEM images for single nanosheets imaged in the [001] direction (Figure 3 e) demonstrate the crystallinity of the sheets, with the expected

DOI: 10.1021/jacs.5b08236
J. Am. Chem. Soc. 2015, 137, 12689–12696

crystallographic lattice reflections. EDX spectrum imaging of a single SnS nanosheet (Figure 3d) confirms undoubtedly that the tin and sulfur signals are colocalized showing an even distribution within the nanosheets and the absence of any impurities (Figure 3g–i). Histograms of the lengths, widths, and aspect ratios of nanosheets imaged by HAADF STEM are presented in the Supporting Information.

Optical Bandgap of SnS Nanosheets. The optical band gap of SnS sol A was determined using UV–vis-NIR absorbance spectroscopy (Figure 4). The absorbance spectrum of the nanosheets has a broad featureless profile, with the onset of absorbance beginning at ca. 1.0 eV. The optical band gap of SnS nanosheets in NMP solution is estimated to be ca. 1.03 eV from the corresponding Tauc plot, and the electronic transition is indirect in nature. There is likely to be systematic error in this value due to the potentially large scattering component associated with sols that contain larger nanosheets.[92] For fractionated SnS sol B, the optical bandgap was determined as 1.65 eV from the corresponding Tauc plot. This band gap energy is significantly higher in energy compared with SnS sol A, due to confinement of the nanosheets in the *c* direction. The accuracy of the latter measurement is expected to be much greater, due to less scattering by thinner nanosheets.

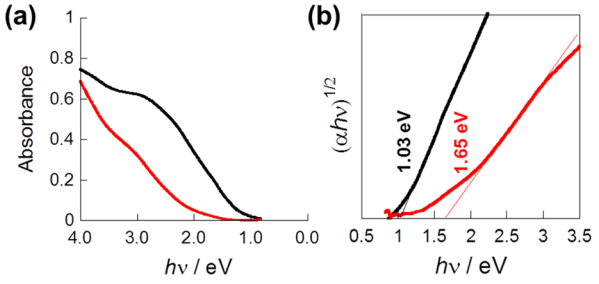

Figure 4. Optical characteristics of SnS nanosheets. (a) UV–vis-NIR absorption spectrum of as-prepared SnS sol A (black line) and from size-selective fractionated SnS sol B (red line). (b) Tauc plot of $(\alpha h\nu)^{1/2}$ vs $h\nu$ from the same data, estimating indirect optical band gaps of 1.03 and 1.65 eV for SnS sol A (black line) and centrifugally fractionated SnS sol B (red line), respectively.

Theoretical Calculations of Nanosheet Semiconducting Properties and Comparison to Experiment. The calculated band structures for bulk SnS, a 10-layer sheet, a SnS bilayer, and a SnS monolayer are shown in Figure 5. In agreement with previous calculations,[93] all structures were found to be indirect semiconductors.

From the calculated density of states curves (Figure 6), it can be concluded that the band gap energy undergoes a systematic and substantial increase of more than 0.5 eV from bulk to bilayer and shows a significant increase for the monolayer.

The evolution of the optical band gap as a function of the thickness can be seen clearly in Figure 7a. This evolution is manifested in the onset of the optical absorption presented in Figure 7b. A comparison of the calculated bulk value to the experimental one of 1.1 eV[95] shows also a good agreement between theory and experiment.

The experimental band gaps determined by optical absorption spectroscopy (red dashed lines, Figure 7a) were overplotted on the optical band gaps calculated by the DFTB approach. It was found that the calculated values matched well for SnS sol A being comprised of around 8 SnS layers on average, though from the AFM results it is likely that this is reflective of the majority species in solution as the nanosheets are polydisperse, and as such should be interpreted with care. On the other hand, SnS sol B, which contains monodisperse nanosheets of mean thickness 4.1 ± 0.2 nm calculated from analysis of AFM images, matches well to the band gap calculated for bilayer nanosheets from the DFTB approach. We

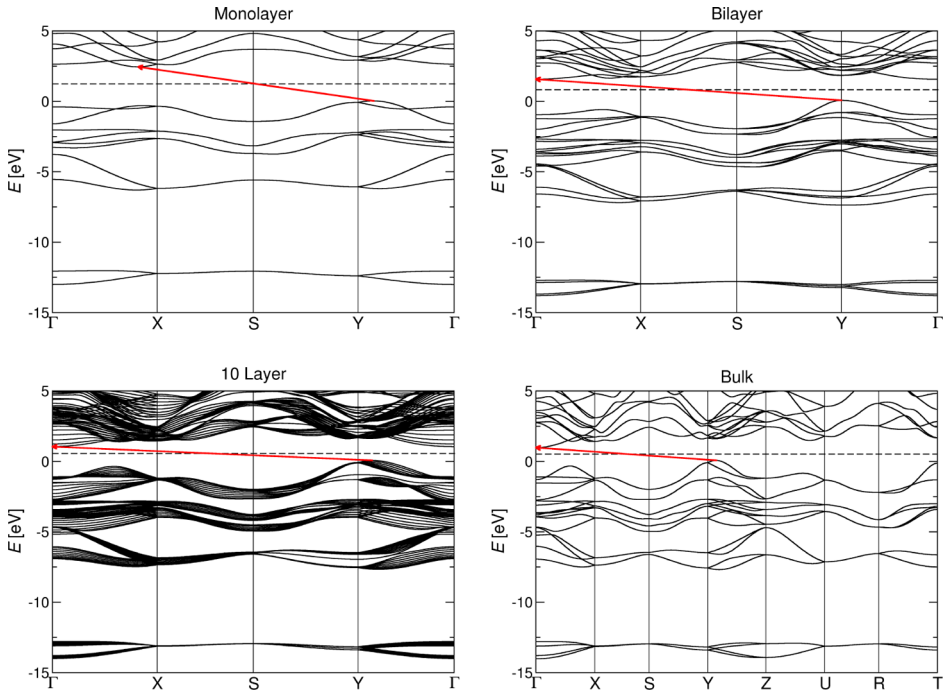

Figure 5. Calculated band structures for monolayer, bilayer, 10-layered multilayer, and bulk SnS. The horizontal dashed lines show the Fermi energies and the red arrows the HOCO–LUCO excitations. HOCO (highest occupied crystal orbital) and LUCO (lowest unoccupied crystal orbital) are the edges of the valence and conduction bands, respectively. The edges of the valence bands have been shifted to zero.

DOI: 10.1021/jacs.5b08236
J. Am. Chem. Soc. 2015, 137, 12689–12696

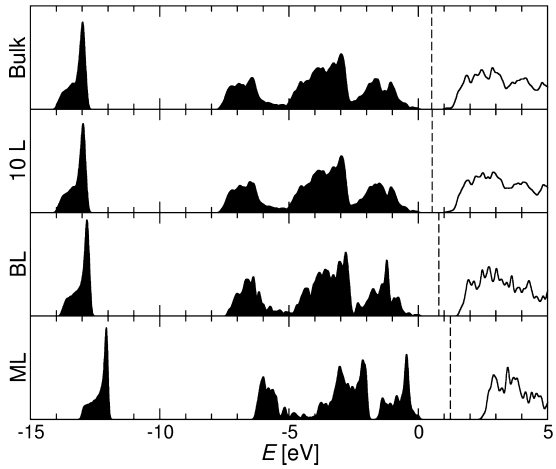

Figure 6. Calculated DOS for monolayer (ML), bilayer (BL), 10-layered multilayer (10 L), and bulk SnS. The Fermi energies are represented by vertical dashed lines. The occupied states are shown by black filled curves and the unoccupied by black lines. A classification of the individual states can be found in Table 2 of Lorenz et al.[94] The edges of the valence bands have been shifted to zero.

suggested that a corrected value for solution processed nanosheets based on measurements in the literature might be on the order of 2 nm/layer, and this matches extremely well to the results from optical absorption experiments and DFTB calculations. We therefore conclude that SnS sol B contains mainly bilayer nanosheets. Interestingly, monolayer SnS nanosheets are not observed at all, suggesting that there is some thermodynamic stability to the bilayer that prevents its further exfoliation to monolayer SnS in solution.

CONCLUSIONS

We have used liquid-phase exfoliation to prepare SnS nanosheets from bulk SnS (Herzenbergite). The nanosheets can be size-selectively fractionated by centrifugation to produce bilayer SnS. Raman spectroscopy shows striking changes upon thinning, with sharpened peak maxima at 164, 190, and 220 cm^{-1}, which can be assigned to the B_{3g}, A_g, and B_{3u} optical modes of SnS. HAADF STEM confirmed the crystallinity of nanosheets and combined with EDX spectrum imaging demonstrated the homogeneity of the elemental distribution of Sn and S within the nanosheets. The DOS and electronic and optical band gaps of bulk to monolayer SnS have been calculated using a quantum chemical DFTB approach. The measured optical properties correspond well to the optical band gaps predicted by quantum chemical DFTB simulations. The band gap of SnS can be tuned by varying the number of SnS layers, which is supported by experiment. This study paves the way for large scale synthesis of main group IV–VI semiconducting nanosheets with a tunable band gap. Scalable process such as the one reported here will be the key to the commercial success of 2-D materials in the future electronics industry.

ASSOCIATED CONTENT

Supporting Information

The Supporting Information is available free of charge on the ACS Publications website at DOI: 10.1021/jacs.5b08236.

Comparison between bulk SnS and exfoliated SnS by Raman spectroscopy, measurement of SnS inter-layer separation from crystallographic data, histograms of length, width, and aspect ratio of nanosheets imaged by HAADF STEM (PDF)

AUTHOR INFORMATION

Corresponding Authors

*david.lewis-4@manchester.ac.uk
*Gotthard.seifert@chemie.tu-dresden.de
*Brian.Derby@manchester.ac.uk
*paul.o'brien@manchester.ac.uk

Author Contributions

‖These authors contributed equally.

Notes

The authors declare no competing financial interest.

ACKNOWLEDGMENTS

P.O.B., J.B., and N.S. thank the Parker family for funding. S.J.H., and E.A.L thank the U.S.A. Defense Threat Reduction Agency (grant number HDTRA1-12-1-0013) as well as NoWNano CDT (EPSRC grant number EP/G03737X/1) for funding support. G.S. and T.L. would like to acknowledge the

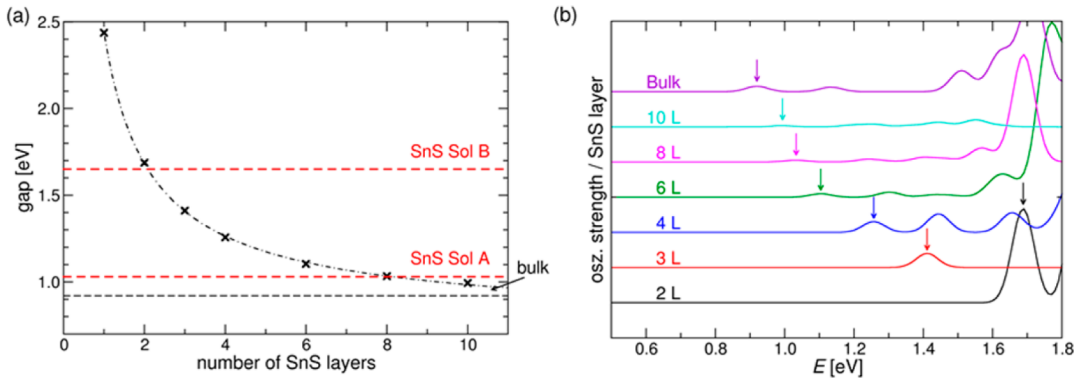

Figure 7. Calculated (a) HOCO–LUCO gap and (b) absorption spectra for SnS multilayers compared with the bulk phase. In figure (a) the bulk value is represented by the black horizontal dashed line and the black crosses show the gap values of the calculated SnS systems. The potential decrease of the gap is indicated by the dash-pointed line. The red dashed lines represent the experimentally determined indirect optical transitions of SnS sols A and B at 1.03 and 1.65 eV, respectively. In (b) the individual SnS structures (*x*L multilayers and bulk) are represented by different colors. The arrows indicate the HOCO–LUCO excitation. The absorption spectrum for single layer SnS (ML) has been omitted, since the lowest excitation occurs only above 2 eV.

DOI: 10.1021/jacs.5b08236
J. Am. Chem. Soc. 2015, 137, 12689–12696

financial support of the DFG (ICENAP project), for computational time provided by ZIH Dresden (project QDSIM). The authors also wish to acknowledge funding support from H.M. Government (U.K.) for the FEI Titan G2 80-200 S/TEM associated with research capability of the Nuclear Advanced Manufacturing Research Centre. Some of the equipment used in this study were provided by the Engineering and Physical Sciences Research Council (*Core Capability in Chemistry*, EPSRC grant number EP/K039547/1).

REFERENCES

(1) Jiang, T.; Ozin, G. A. *J. Mater. Chem.* **1998**, *8*, 1099.
(2) Tremel, W.; Hoffmann, R. *Inorg. Chem.* **1987**, *26*, 118.
(3) Hultgren, R.; Gingrich, N. S.; Warren, B. E. *J. Chem. Phys.* **1935**, *3*, 351.
(4) Madelung, O. *Semiconductors - Basic Data*, 2nd ed.; Springer-Verlag: Berlin, 1996.
(5) Sinsermsuksakul, P.; Sun, L.; Lee, S. W.; Park, H. H.; Kim, S. B.; Yang, C.; Gordon, R. G. *Adv. Energy Mater.* **2014**, *4*, 1400496.
(6) Loferski, J. J. *J. Appl. Phys.* **1956**, *27*, 777.
(7) Kevin, P.; Lewis, D. J.; Raftery, J.; Malik, M. A.; O'Brien, P. *J. Cryst. Growth* **2015**, *415*, 93.
(8) Ramasamy, K.; Kuznetsov, V. L.; Gopal, K.; Malik, M. A.; Raftery, J.; Edwards, P. P.; O'Brien, P. *Chem. Mater.* **2013**, *25*, 266.
(9) Bade, B. P.; Garje, S. S.; Niwate, Y. S.; Afzaal, M.; O'Brien, P. *Chem. Vap. Deposition* **2008**, *14*, 292.
(10) Hibbert, T. G.; Mahon, M. F.; Molloy, K. C.; Price, L. S.; Parkin, I. P. *J. Mater. Chem.* **2001**, *11*, 469.
(11) Kana, A. T.; Hibbert, T. G.; Mahon, M. F.; Molloy, K. C.; Parkin, I. P.; Price, L. S. *Polyhedron* **2001**, *20*, 2989.
(12) Parkin, I. P.; Price, L. S.; Hardy, A. M. E.; Clark, R. J. H.; Hibbert, T. G.; Molloy, K. C. *J. Phys. IV France* **1999**, *9*, 403.
(13) Price, L. S.; Parkin, I. P.; Field, M. N.; Hardy, A. M. E.; Clark, R. J. H.; Hibbert, T. G.; Molloy, K. C. *J. Mater. Chem.* **2000**, *10*, 527.
(14) Price, L. S.; Parkin, I. P.; Hibbert, T. G.; Molloy, K. C. *Chem. Vap. Deposition* **1998**, *4*, 222.
(15) Sanchez-Juarez, A.; Tiburcio-Silver, A.; Ortiz, A. *Thin Solid Films* **2005**, *480*, 452.
(16) Gao, C.; Shen, H. *Thin Solid Films* **2012**, *520*, 3523.
(17) Tanusevski, A. *Semicond. Sci. Technol.* **2003**, *18*, 501.
(18) Cheng, S. Y.; Chen, G. A.; Chen, Y. Q.; Huang, C. C. *Opt. Mater.* **2006**, *29*, 439.
(19) Ichimura, M.; Takeuchi, K.; Ono, Y.; Arai, E. *Thin Solid Films* **2000**, *361*, 98.
(20) Arora, S. K.; Patel, D. H.; Agarwal, M. K. *J. Cryst. Growth* **1993**, *131*, 268.
(21) Arora, S. K.; Patel, D. H.; Agarwal, M. K. *J. Mater. Sci.* **1994**, *29*, 3979.
(22) Kim, J. Y.; George, S. M. *J. Phys. Chem. C* **2010**, *114*, 17597.
(23) Sinsermsuksakul, P.; Heo, J.; Noh, W.; Hock, A. S.; Gordon, R. G. *Adv. Energy Mater.* **2011**, *1*, 1116.
(24) Calixto-Rodriguez, M.; Martinez, H.; Sanchez-Juarez, A.; Campos-Alvarez, J.; Tiburcio-Silver, A.; Calixto, M. E. *Thin Solid Films* **2009**, *517*, 2497.
(25) Reddy, N. K.; Reddy, K. T. R. *Thin Solid Films* **1998**, *325*, 4.
(26) Sudha, M.; Duraisamy, P. *Optoelectron. Adv. Mater.-Rapid Commun.* **2012**, *6*, 999.
(27) Ray, S. C.; Karanjai, M. K.; DasGupta, D. *Thin Solid Films* **1999**, *350*, 72.
(28) de Kergommeaux, A.; Faure-Vincent, J.; Pron, A.; de Bettignies, R.; Malaman, B.; Reiss, P. *J. Am. Chem. Soc.* **2012**, *134*, 11659.
(29) Deng, Z. T.; Han, D. R.; Liu, Y. *Nanoscale* **2011**, *3*, 4346.
(30) Hickey, S. G.; Waurisch, C.; Rellinghaus, B.; Eychmueller, A. *J. Am. Chem. Soc.* **2008**, *130*, 14978.
(31) Koktysh, D. S.; McBride, J. R.; Rosenthal, S. J. *Nanoscale Res. Lett.* **2007**, *2*, 144.
(32) Ning, J.; Men, K.; Xiao, G.; Wang, L.; Dai, Q.; Zou, B.; Liu, B.; Zou, G. *Nanoscale* **2010**, *2*, 1699.
(33) Patra, B. K.; Sarkar, S.; Guria, A. K.; Pradhan, N. *J. Phys. Chem. Lett.* **2013**, *4*, 3929.
(34) Ren, L.; Jin, Z.; Wang, W.; Liu, H.; Lai, J.; Yang, J.; Hong, Z. *Appl. Surf. Sci.* **2011**, *258*, 1353.
(35) Xu, Y.; Al-Salim, N.; Bumby, C. W.; Tilley, R. D. *J. Am. Chem. Soc.* **2009**, *131*, 15990.
(36) Lewis, D. J.; Kevin, P.; Bakr, O.; Muryn, C. A.; Malik, M. A.; O'Brien, P. *Inorg. Chem. Front.* **2014**, *1*, 577.
(37) Geim, A. K.; Novoselov, K. S. *Nat. Mater.* **2007**, *6*, 183.
(38) Novoselov, K. S.; Geim, A. K.; Morozov, S. V.; Jiang, D.; Zhang, Y.; Dubonos, S. V.; Grigorieva, I. V.; Firsov, A. A. *Science* **2004**, *306*, 666.
(39) Novoselov, K.; Jiang, D.; Schedin, F.; Booth, T. J.; Khotkevich, V. V.; Morosov, S. V.; Geim, A. K. *Proc. Natl. Acad. Sci. U. S. A.* **2005**, *102*, 10451.
(40) Miro, P.; Audiffred, M.; Heine, T. *Chem. Soc. Rev.* **2014**, *43*, 6537.
(41) Lee, C.; Wei, X.; Kysar, J. W.; Hone, J. *Science* **2008**, *321*, 385.
(42) Novoselov, K. S.; Geim, A. K.; Morozov, S. V.; Jiang, D.; Katsnelson, M. I.; Grigorieva, I. V.; Dubonos, S. V.; Firsov, A. A. *Nature* **2005**, *438*, 197.
(43) Mak, K. F.; Lee, C.; Hone, J.; Shan, J.; Heinz, T. F. *Phys. Rev. Lett.* **2010**, *105*, 136805.
(44) Butler, S. Z.; Hollen, S. M.; Cao, L.; Cui, Y.; Gupta, J. A.; Gutiérrez, H. R.; Heinz, T. F.; Hong, S. S.; Huang, J.; Ismach, A. F.; Johnston-Halperin, E.; Kuno, M.; Plashnitsa, V. V.; Robinson, R. D.; Ruoff, R. S.; Salahuddin, S.; Shan, J.; Shi, L.; Spencer, M. G.; Terrones, M.; Windl, W.; Goldberger, J. E. *ACS Nano* **2013**, *7*, 2898.
(45) Liu, H.; Neal, A. T.; Zhu, Z.; Luo, Z.; Xu, X.; Tománek, D.; Ye, P. D. *ACS Nano* **2014**, *8*, 4033.
(46) Xia, F.; Wang, H.; Jia, Y. *Nat. Commun.* **2014**, *5*, 4458.
(47) Fei, R.; Yang, L. *Nano Lett.* **2014**, *14*, 2884.
(48) Liu, H.; Du, Y.; Deng, Y.; Ye, P. D. *Chem. Soc. Rev.* **2015**, *44*, 2732.
(49) Wood, J. D.; Wells, S. A.; Jariwala, D.; Chen, K.-S.; Cho, E.; Sangwan, V. K.; Liu, X.; Lauhon, L. J.; Marks, T. J.; Hersam, M. C. *Nano Lett.* **2014**, *14*, 6964.
(50) Doganov, R. A.; O'Farrell, E. C. T.; Koenig, S. P.; Yeo, Y.; Ziletti, A.; Carvalho, A.; Campbell, D. K.; Coker, D. F.; Watanabe, K.; Taniguchi, T.; Neto, A. H. C.; Ozyilmaz, B. *Nat. Commun.* **2015**, *6*, 6647.
(51) Hanlon, D.; Backes, C.; Doherty, E.; Cucinotta, C. S.; Berner, N. C.; Boland, C.; Lee, K.; Lynch, P.; Gholamvand, Z.; Harvey, A.; Zhang, S.; Wang, K.; Sanvito, S.; O'Regan, D. D.; Duesberg, G. S.; Nicolosi, V.; Coleman, J. N. *arXiv* **2015**, *1501*, 01881.
(52) Reina, A.; Jia, X. T.; Ho, J.; Nezich, D.; Son, H. B.; Bulovic, V.; Dresselhaus, M. S.; Kong, J. *Nano Lett.* **2009**, *9*, 30.
(53) Huang, C.-C.; Al-Saab, F.; Wang, Y.; Ou, J.-Y.; Walker, J. C.; Wang, S.; Gholipour, B.; Simpson, R. E.; Hewak, D. W. *Nanoscale* **2014**, *6*, 12792.
(54) Hernandez, Y.; Lotya, M.; Rickard, D.; Bergin, S. D.; Coleman, J. N. *Langmuir* **2010**, *26*, 3208.
(55) Sresht, V.; Pádua, A. A. H.; Blankschtein, D. *ACS Nano* **2015**, *9*, 8255.
(56) Coleman, J. N.; Lotya, M.; O'Neill, A.; Bergin, S. D.; King, P. J.; Khan, U.; Young, K.; Gaucher, A.; De, S.; Smith, R. J.; Shvets, I. V.; Arora, S. K.; Stanton, G.; Kim, H.-Y.; Lee, K.; Kim, G. T.; Duesberg, G. S.; Hallam, T.; Boland, J. J.; Wang, J. J.; Donegan, J. F.; Grunlan, J. C.; Moriarty, G.; Shmeliov, A.; Nicholls, R. J.; Perkins, J. M.; Grieveson, E. M.; Theuwissen, K.; McComb, D. W.; Nellist, P. D.; Nicolosi, V. *Science* **2011**, *331*, 568.
(57) Hernandez, Y.; Nicolosi, V.; Lotya, M.; Blighe, F. M.; Sun, Z.; De, S.; McGovern, I. T.; Holland, B.; Byrne, M.; Gun'Ko, Y. K.; Boland, J. J.; Niraj, P.; Duesberg, G.; Krishnamurthy, S.; Goodhue, R.; Hutchison, J.; Scardaci, V.; Ferrari, A. C.; Coleman, J. N. *Nat. Nanotechnol.* **2008**, *3*, 563.
(58) O'Neill, A.; Khan, U.; Coleman, J. N. *Chem. Mater.* **2012**, *24*, 2414.

DOI: 10.1021/jacs.5b08236
J. Am. Chem. Soc. 2015, 137, 12689−12696

(59) Paton, K. R.; Varrla, E.; Backes, C.; Smith, R. J.; Khan, U.; O'Neill, A.; Boland, C.; Lotya, M.; Istrate, O. M.; King, P.; Higgins, T.; Barwich, S.; May, P.; Puczkarski, P.; Ahmed, I.; Moebius, M.; Pettersson, H.; Long, E.; Coelho, J. o.; O'Brien, S. E.; McGuire, E. K.; Sanchez, B. M.; Duesberg, G. S.; McEvoy, N.; Pennycook, T. J.; Downing, C.; Crossley, A.; Nicolosi, V.; Coleman, J. N. *Nat. Mater.* **2014**, *13*, 624.
(60) Varrla, E.; Backes, C.; Paton, K. R.; Harvey, A.; Gholamvand, Z.; McCauley, J.; Coleman, J. N. *Chem. Mater.* **2015**, *27*, 1129.
(61) Savjani, N.; Lewis, E. A.; Pattrick, R. A. D.; Haigh, S. J.; O'Brien, P. *RSC Adv.* **2014**, *4*, 35609.
(62) Lewis, D. J.; Tedstone, A. A.; Zhong, X. L.; Lewis, E. A.; Rooney, A.; Savjani, N.; Brent, J. R.; Haigh, S. J.; Burke, M. G.; Muryn, C. A.; Raftery, J. M.; Warrens, C.; West, K.; Gaemers, S.; O'Brien, P. *Chem. Mater.* **2015**, *27*, 1367.
(63) Brent, J. R.; Savjani, N.; Lewis, E. A.; Haigh, S. J.; Lewis, D. J.; O'Brien, P. *Chem. Commun.* **2014**, *50*, 13338.
(64) Yasaei, P.; Kumar, B.; Foroozan, T.; Wang, C.; Asadi, M.; Tuschel, D.; Indacochea, J. E.; Klie, R. F.; Salehi-Khojin, A. *Adv. Mater.* **2015**, *27*, 1887.
(65) Kang, J.; Wood, J. D.; Wells, S. A.; Lee, J.-H.; Liu, X.; Chen, K.-S.; Hersam, M. C. *ACS Nano* **2015**, *9*, 3596.
(66) Zhang, Y.; Lu, J.; Shen, S.; Xu, H.; Wang, Q. *Chem. Commun.* **2011**, *47*, 5226.
(67) Zhu, H. L.; Yang, D. R.; Ji, Y. J.; Zhang, H.; Shen, X. F. *J. Mater. Sci.* **2005**, *40*, 591.
(68) Biswas, S.; Kar, S.; Chaudhuri, S. *Appl. Surf. Sci.* **2007**, *253*, 9259.
(69) Sohila, S.; Rajalakshmi, M.; Muthamizhchelvan, C.; Kalavathi, S.; Ghosh, C.; Divakar, R.; Venkiteswaran, C. N.; Muralidharan, N. G.; Arora, A. K.; Mohandas, E. *Mater. Lett.* **2011**, *65*, 1148.
(70) Salavati-Niasari, M.; Davar, F. *J. Alloys Compd.* **2010**, *492*, 570.
(71) Acharya, S.; Das, B.; Thupakula, U.; Ariga, K.; Sarma, D. D.; Israelachvili, J.; Golan, Y. *Nano Lett.* **2013**, *13*, 409.
(72) Niehaus, T. A.; Suhai, S.; Della Sala, F.; Lugli, P.; Elstner, M.; Seifert, G.; Frauenheim, T. *Phys. Rev. B: Condens. Matter Mater. Phys.* **2001**, *63*, 085108.
(73) Porezag, D.; Frauenheim, T.; Kohler, T.; Seifert, G.; Kaschner, R. *Phys. Rev. B: Condens. Matter Mater. Phys.* **1995**, *51*, 12947.
(74) Seifert, G. *J. Phys. Chem. A* **2007**, *111*, 5609.
(75) Seifert, G.; Joswig, J.-O. *Wiley Interdiscip. Rev. Comp. Mol. Sci.* **2012**, *2*, 456.
(76) Seifert, G.; Porezag, D.; Frauenheim, T. *Int. J. Quantum Chem.* **1996**, *58*, 185.
(77) Hohenburg, P.; Kohn, W. *Phys. Rev.* **1964**, *136*, B864.
(78) Kohn, W.; Sham, L. J. *Phys. Rev.* **1965**, *140*, 1133.
(79) Gomes, L. C.; Carvalho, A. *Phys. Rev. B: Condens. Matter Mater. Phys.* **2015**, *92*, 085406.
(80) Koester, A. M.; Geudtner, G.; Goursot, A.; Heine, T.; Vela, A.; Salahub, D.; Patchkovskii, S. *deMon Software*; NRC: Ottawa, Canada, 2004.
(81) Perdew, J. P.; Burke, K.; Ernzerhof, M. *Phys. Rev. Lett.* **1996**, *77*, 3865.
(82) Soler, J. M.; Artacho, E.; Gale, J. D.; Garcia, A.; Junquera, J.; Ordejon, P.; Sanchez-Portal, D. *J. Phys.: Condens. Matter* **2002**, *14*, 2745.
(83) Wiedemeier, H.; Schnering, H. G. V. *Z. Kristallogr.* **1978**, *148*, 295.
(84) Monkhorst, H. J.; Pack, J. D. *Phys. Rev. B* **1976**, *13*, 5188.
(85) Yang, H.; Withers, F.; Gebremedhn, E.; Lewis, E. A.; Britnell, L.; Felten, A.; Palermo, V.; Haigh, S. J.; Beljonne, D.; Casiraghi, C. *2D Mater.* **2014**, *1*, 011012.
(86) Yang, H.; Hernandez, Y.; Schlierf, A.; Felten, A.; Eckmann, A.; Johal, S.; Louette, P.; Pireaux, J. J.; Feng, X.; Mullen, K.; Palermo, V.; Casiraghi, C. *Carbon* **2013**, *53*, 357.
(87) Schlierf, A.; Yang, H.; Gebremedhn, E.; Treossi, E.; Ortolani, L.; Chen, L.; Minoia, A.; Morandi, V.; Samori, P.; Casiraghi, C.; Beljonne, D.; Palermo, V. *Nanoscale* **2013**, *5*, 4205.
(88) Chandrasekhar, H. R.; Humphreys, R. G.; Zwick, U.; Cardona, M. *Phys. Rev. B* **1977**, *15*, 2177.
(89) Price, L. S.; Parkin, I. P.; Hardy, A. M. E.; Clark, R. J. H.; Hibbert, T. G.; Molloy, K. C. *Chem. Mater.* **1999**, *11*, 1792.
(90) Kang, J.-G.; Ko, Y.-D.; Choi, K. J.; Park, J.-G.; Kim, D.-W. *Appl. Phys. A: Mater. Sci. Process.* **2011**, *103*, 505.
(91) Molina-Sanchez, A.; Wirtz, L. *Phys. Rev. B: Condens. Matter Mater. Phys.* **2011**, *84*, 155413.
(92) Backes, C.; Smith, R. J.; McEvoy, N.; Berner, N. C.; McCloskey, D.; Nerl, H. C.; O'Neill, A.; King, P. J.; Higgins, T.; Hanlon, D.; Scheuschner, N.; Maultzsch, J.; Houben, L.; Duesberg, G. S.; Donegan, J. F.; Nicolosi, V.; Coleman, J. N. *Nat. Commun.* **2014**, *5*, 4576.
(93) Tritsaris, G. A.; Malone, B. D.; Kaxiras, E. *J. Appl. Phys.* **2013**, *113*, 233507.
(94) Lorenz, T.; Joswig, J.-O.; Seifert, G. *Semicond. Sci. Technol.* **2014**, *29*, 064006.
(95) Albers, W.; Haas, C.; Vandermaesen, F. *J. Phys. Chem. Solids* **1960**, *15*, 306.

DOI: 10.1021/jacs.5b08236
J. Am. Chem. Soc. 2015, 137, 12689−12696